Design, Construction and Operation of an Automated Drilling Rig for the DSATS University Competition

Student Team:
Roman Shor, Runqi Han, Adrian Ambrus, Parham Pournazari, Can Pehlivanturk

Advisors:
Eric van Oort, Pradeep Ashok, and Mitch Pryor

The University of Texas at Austin

Abstract

SPE DSATS has organized an annual competition for universities around the world to design, construct and control autonomous laboratory scale drilling machines to further innovation in the drilling automation space. The paper describes the design choices, control methodologies and results obtained by the University of Texas at Austin during the inaugural 2015 contest. The team designed a light-weight and modular rig that maximized power output and utilized the large sample provided by DSATS as an inertial and stabilizing base support. A continuous chain-driven draw works provided axial actuation while an AC gear motor provided drill string rotation. A closed-loop fluid circulation system facilitated removal of cuttings as well as cooling and lubrication of the drill bit. Drilling was primarily conducted by closed-loop weight on bit control, through the use of a sliding mode controller, complete with set point changes based on lithology detection. The final design successfully drilled a total of 30.48 centimeters through the sample, with data being presented in real-time as well as stored for further analysis.

Introduction

The Society of Petroleum Engineers (SPE), through its Drilling Systems Automation Technical Session (DSATS) has organized a competition for university students with the goal to build an autonomous machine exhibiting functionality of a modern-day drilling rig. This machine should be capable of autonomously drilling a vertical hole through a 60x60x60 cm rock sample provided by the DSATS committee. The sample, pictured in **Figure 1**, consists of two layers of Berea sandstone epoxied to a granite layer. Teams accepted into the competition were given $10,000 to build the selected design and DSATS also supplied the drill pipe and drill bit, along with tool joints and a cross-over sub. The design specifications for the competition are shown in **Table 1** below.

Table 1. Design specifications for DSATS competition.

Maximum rig height	2 m
Maximum power	2.5 hp
Maximum WOB	50 lbs
Drill bit (provided by DSATS)	PDC micro-bit 1.125" diameter
Drill pipe (provided by DSATS)	Aluminum 3003 H14 with 3/8" OD, 0.016" wall thickness
Maximum cost	$15,000 (DSATS to fund $10,000)
Sensors	Continuous measurement of weight on bit
Other	Bit/machinery to be cooled with air/water

Laboratory-scale automatic and semi-automatic drilling rigs have previously been designed for research purposes. Ersoy (2003) described an automatically controlled rig applying constant power to a PDC bit. The rig was used to drill through a variety of lithologies, with mechanical specific energy (MSE) being used to evaluate drilling performance. Khulief et al. (2009) used an experimental setup capable of simulating different drilling vibrational modes. Their setup consisted of a variable speed motor providing drill string rotation, an electromagnetic brake for inducing stick-slip conditions and a shaker for exciting bit bounce. Another laboratory rig, capable of producing torques as high as 1900 N·m and weight on bit up to 150 kN, was used by Lund et al. (2009) to investigate PDC bearing and cutter performance while drilling through Barre granite. Esmaeili et al. (2012) described a small-scale laboratory rig that is able to drill 30x30x30 cm concrete samples but with a higher weight on bit than allowed for this competition. Their rig was used primarily for experimental evaluation of formation mechanical properties via drilling dysfunctions and MSE trends.

The University of Texas at Austin, through its Drilling and Rig Automation Group, designed the "nanoRig" pictured in **Figure 2**. Detailed description of the mechanical design, actuation, sensing and control architecture are provided in the following sections. In all the prior art discussed above, there were no stringent design constraints, such as the ones imposed for the DSATS competition. Thus, the main focus of our design was placed on limiting potential damage to the drill pipe and drill bit, at the expense of drilling optimization. As a result, the control system became a crucial part of the design, as well as the ability to detect formation changes and potential drilling problems.

Figure 1. Materials provided by DSATS: rock sample (left); drill string assembly (right).

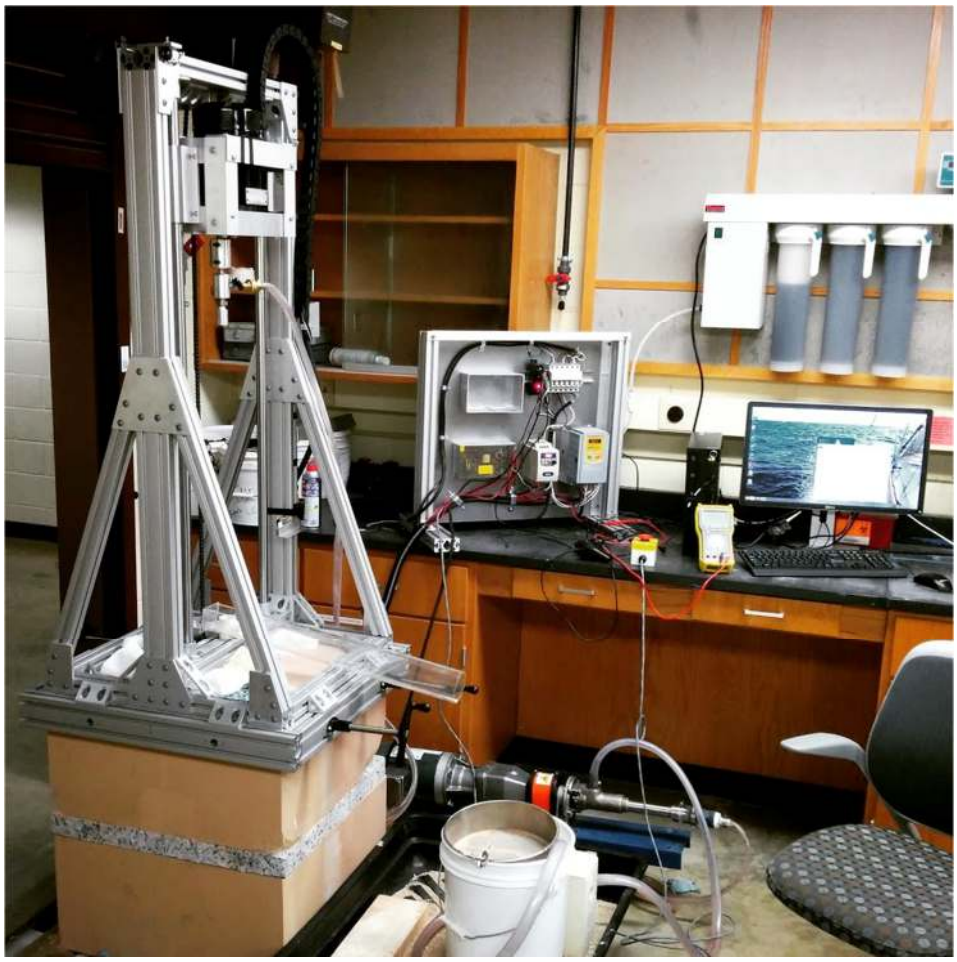

Figure 2. The University of Texas at Austin nanoRig.

Mechanical Design

Structural Support

The team went through several design iterations before settling on the final rig design. One of the early ideas, portrayed on the left of **Figure 3**, was to mount the rig over the sample, and use outriggers that both grip the sample when engaged and provide horizontal balance. A sample-mounted rig could use the sample as an inertial mass to absorb vibration, as a structural support to maintain verticality, and as a way to reduce rig size since floor support is not necessary. In the final design, shown on the right side of **Figure 3,** the outriggers were discarded, and instead the rig base would be attached to the sample using eight screw clamps, two on each side of the rig. The design of the frame also went through several iterations, from welded steel beams to 80/20 modular aluminum framing in the final design. The decision to use 80/20 was mainly due to the desire to have a lightweight and easy to assemble frame. The transverse beam on the base of the rig serves as structural support and also provides a pilot hole, having the center of the beam drilled and a PVC tee pipe installed on it. The side outlet of the tee serves as a return line for the drilling fluid exiting the drill bit nozzles.

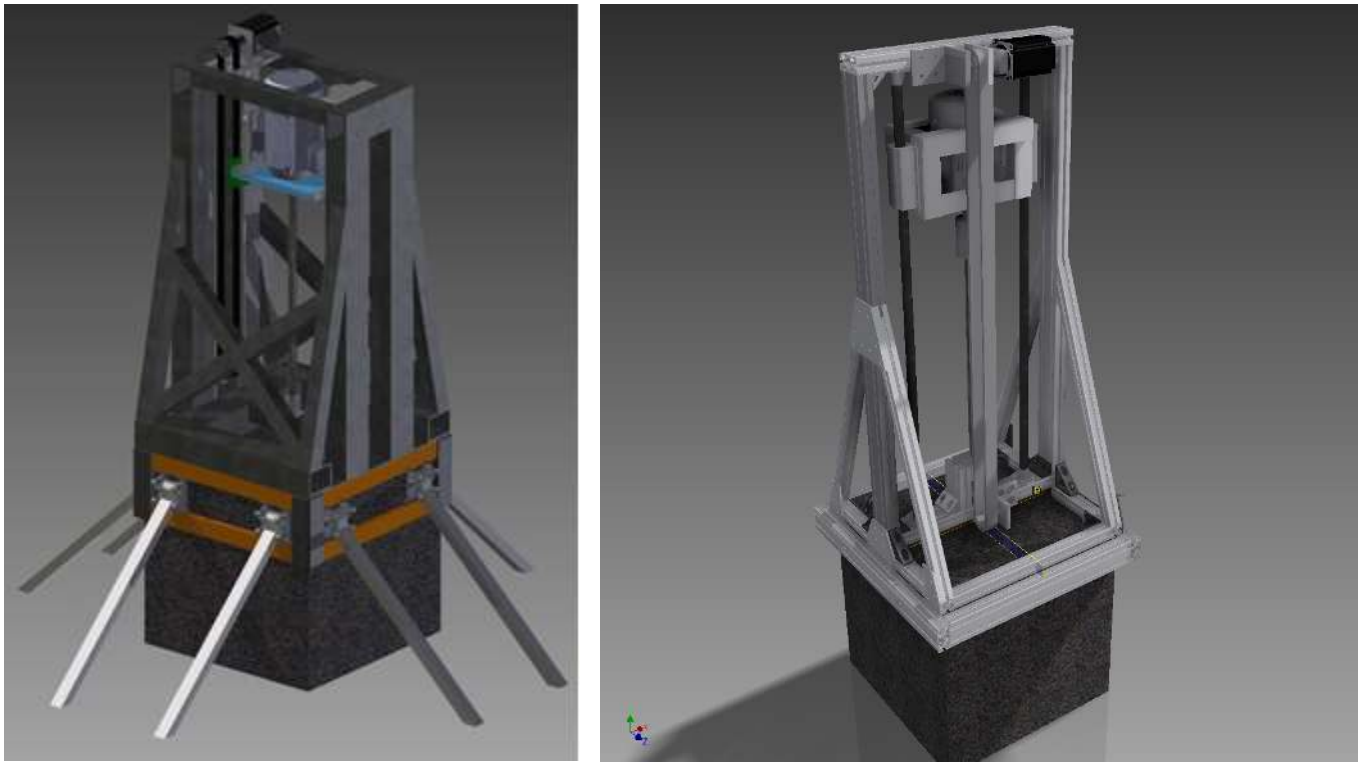

Figure 3. CAD model of original design (left) and final design (right).

Rotational Actuation

A top drive design was chosen for the rotational actuation. The initial choice was a 2 hp geared AC motor, but upon revealing the drill pipe specifications, the motor had to be reconsidered. Ultimately, the team purchased a Bodine Electric 48R-F Series Parallel Shaft AC Gearmotor rated at 0.5 hp with an integral 5:1 gearbox providing 56 lb-in of torque at 340 rpm. The motor is housed inside a carriage constructed from steel L-beams bolted together. The top drive also provides the weight on bit, the gearmotor alone weighing 26 lbs. A swivel is coupled to the motor shaft, and the side port on the swivel enables fluid circulation inside the drill pipe. A 3-axis accelerometer is mounted on the top drive carriage, allowing the diagnosis of axial and transverse vibrations encountered during the rig operation.

Hoisting System

The hoisting system, pictured in **Figure 4**, comprises a Schneider MDrive 23 Plus stepper motor with a 10:1 gearbox, a Deltran power off servo brake, and a chain drive passing over a sprocket. The stepper provides a holding torque of 200 oz·in, which when coupled to the gearbox, provides ample holding torque to maintain drawworks height. A liquid cooling system with a fan is also mounted on the top side of the rig, in order to prevent the stepper from over heating. Stepper position is measured using an encoder with a resolution of 2048 counts/resolution. The top drive carriage (**Figure 5**) is attached to linear ball bearings which slide on hardened steel rods. A Futek S-beam load cell is mounted on the side of the top drive carriage in between the ends of the chain. This allows for continuous reading of the tension in the chain, which can be easily translated into WOB. Mechanical end stops are used to limit the vertical motion of the top drive carriage to a travel range of 81 cm. These end stops are wired into the stepper drive to send stop commands to the motor upon mechanical contact with the top drive carriage.

Figure 4. Hoisting system: stepper motor, brake and chain (left); cooling unit (right).

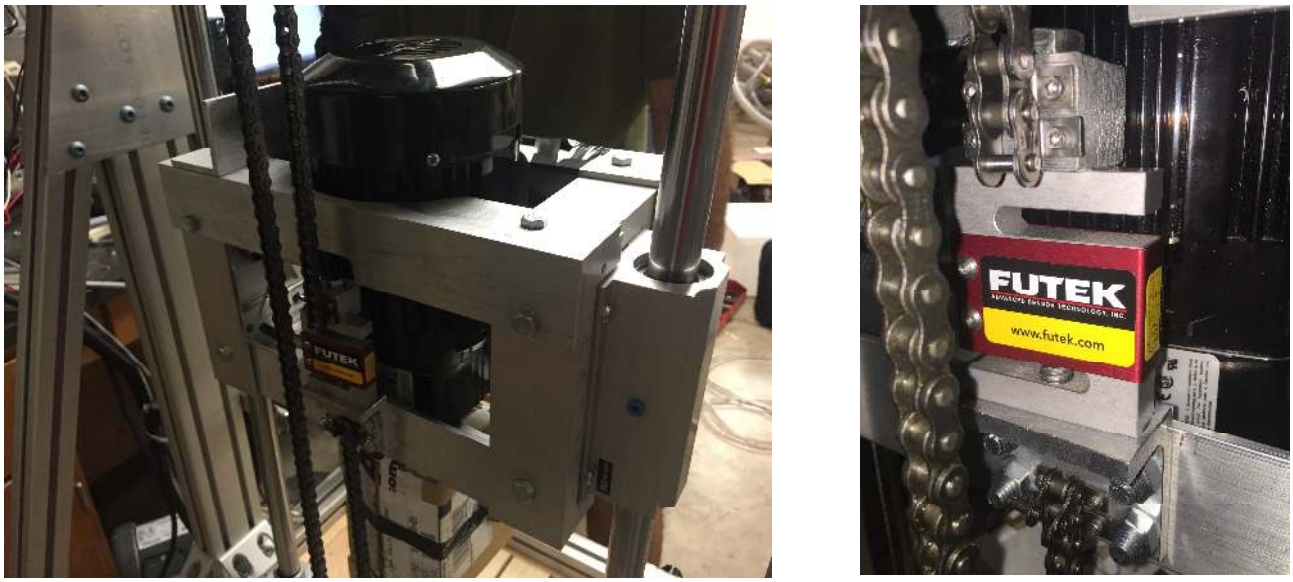

Figure 5. Top drive carriage (left); close-up of S-beam load cell (right).

Fluid Circulation

While not explicitly required by the DSATS competition, a closed loop fluid circulation system was added to the design to facilitate removal of drill cuttings and provide cooling and lubrication to the bit. The circulation system consists of a pump, hose, swivel, the inside of the drill pipe, drill bit nozzles and fluids return line, terminating in a bucket with a sieve emulating a shale shaker (see **Figure 6**). Tap water, serving as the drilling fluid, is pumped from the bucket through the hose, and re-enters the bucket through the return line, resulting in a closed-loop circulation system. A rubber plunger together with silicone and spray foam were used to seal the annulus and prevent leaks in the system which was necessary since the testing was conducted in an indoor environment. Once the upper sandstone layer was drilled, significant losses began since the sandstone and granite had an imperfect epoxy bonding layer, forcing frequent refilling of the mud bucket.

Figure 6. Pump, mud bucket and fluid returns line (left); swivel (right).

Design Calculations

Several high-level mechanical design calculations were performed to verify the structural integrity of the rig. One of the scenarios we modeled was the case of an instantaneous stall of the top drive (e.g., due to an overcurrent in the AC motor). A worst-case scenario of rotational velocity suddenly dropping to zero from the maximum value of 340 rpm, results in a torsional load of $511 N \cdot m$ (see **Appendix A** for detailed calculations**).** The combined weight of the rig and sample is roughly 1500 lbs (6672 N), which generates a rotational moment of $6672 N \times 0.3\, m = 2002\, N \cdot m$ about the clamping points. This value is sufficient to prevent the rig from tipping over in the case of the shock load described above.

We were also interested in avoiding bending of the steel rods guiding the top drive carriage. The equivalent force generated by the shock load at the bearing (assuming no losses/dissipation in the top drive components) is

$$P = \frac{|T_{avg}|}{d} = \frac{511 N \cdot m}{0.19\, m} = 2690\, N$$

From Euler-Bernoulli beam theory (Gere and Goodno, 2008), the maximum bending and shear stresses in the rods are

$$\sigma_{b,max} = \frac{128PL}{27\pi d^3}; \tau_{max} = \frac{16P}{3\pi d^2}$$

with L the length of the rod and d its diameter.

Plugging in values, for L = 1.2 m, d = 2.54 cm and P = 2690 N we have (see **Appendix B** for detailed derivations).

$$\sigma_{b,\max} = 297\ MPa$$
$$\tau_{max} = 7.08\ MPa$$

For case hardened steel, $\sigma_y = 610\ MPa$ and $\tau_y = 0.58\sigma_y = 354\ MPa$ which gives a safety factor of 2.05 for yield due to bending and a safety factor of 50 for yielding in shear.

Operational Limits

During regular operation, the drill pipe is loaded in torsion and compression. The imperfections in the alignment of the motor, the drill pipe, bit and the wellbore are expected to create eccentricity in the axial loading. This in turn will create a bending moment that is fully alternating therefore the fatigue failure of the drill pipe is also considered.

In compression, the drill pipe is considered a long column with eccentric loading and the critical load for unstable buckling is the main limiting factor on the axial force or WOB. First, the Euler column formula is considered with fixed-fixed end condition constant recommended values (Budynas et al., 2014). Moreover, similar to fatigue failure calculations, the secant column formula with eccentric loading is considered. The maximum eccentricity is assumed to be equal to the diameter of the bit. A safety factor of 2 is used and the minimum allowable axial load from the two formulas is chosen as the WOB limit.

The allowable limits for torsion are out of reach for regular drilling operation, however if a stuck pipe situation occurs, the inertia of the motor is more than enough to exceed the torsion limits leading to a twist off. This is difficult to manage and detect preemptively as the torque is estimated from the VFD current and the torque caused by the motor inertia itself is not observable from current measurements. The best course of action is to prevent stuck pipe altogether by having good fluid circulation.

The aluminum drill pipe poses a limitation on the design against fatigue as aluminum alloys do not have an endurance limit and will always fail if a sufficient number of load cycles are applied (Campbell et al., 2008). The goal is to operate through the projected number of cycles without failure. The cycle limit is roughly approximated as 500,000 which stems from 24 hours of drilling at max RPM of 340 (motor RPM is limited by the hardware). Assuming fully reversed loading with maximum allowable eccentricity we are inside the allowable cycles to failure (Yahr, 1997) , however changes in eccentricity and WOB will lead to higher bending stress which may result in premature failure in fatigue. The calculated maximum allowable limits on control parameters are presented in **Table 2**.

Table 2 - Maximum allowable limits on control parameters.

Motor RPM	340
Motor Torque before twist off	5 Nm
WOB	15 lbf
Eccentricity	15 mm

Hardware and Software Design

The top drive motor is controlled using a Parker AC10 Variable Frequency Drive (VFD). A TECO EV JNEV2P5H1 VFD is used for the pump. The VFD's and stepper drive are powered from a 230 VAC source with individual circuit breakers for the stepper motor, AC motor and pump (see **Figure 7**). E-stops for the VFD's and brake are also wired into the electrical console. The top drive VFD allows continuous measurements of current and frequency, which can be easily converted into torque and rotational speed, respectively. A NI USB-6003 is used for obtaining measurements from the load cell and accelerometer, sampled continuously at a rate of 1000 Hz.

Figure 8 shows a basic overview of the control architecture. A basic dual-core workstation is used to interface all the hardware components and provides low-level control using C and mex functions, while the supervisory control and graphical user interface are handled in Matlab. The supervisory control loop runs separate threads for the VFD's, stepper and DAQ. Through the interface shown in Figure 9, the user can monitor the system status and drilling parameters, and can terminate the execution of the program at any time.

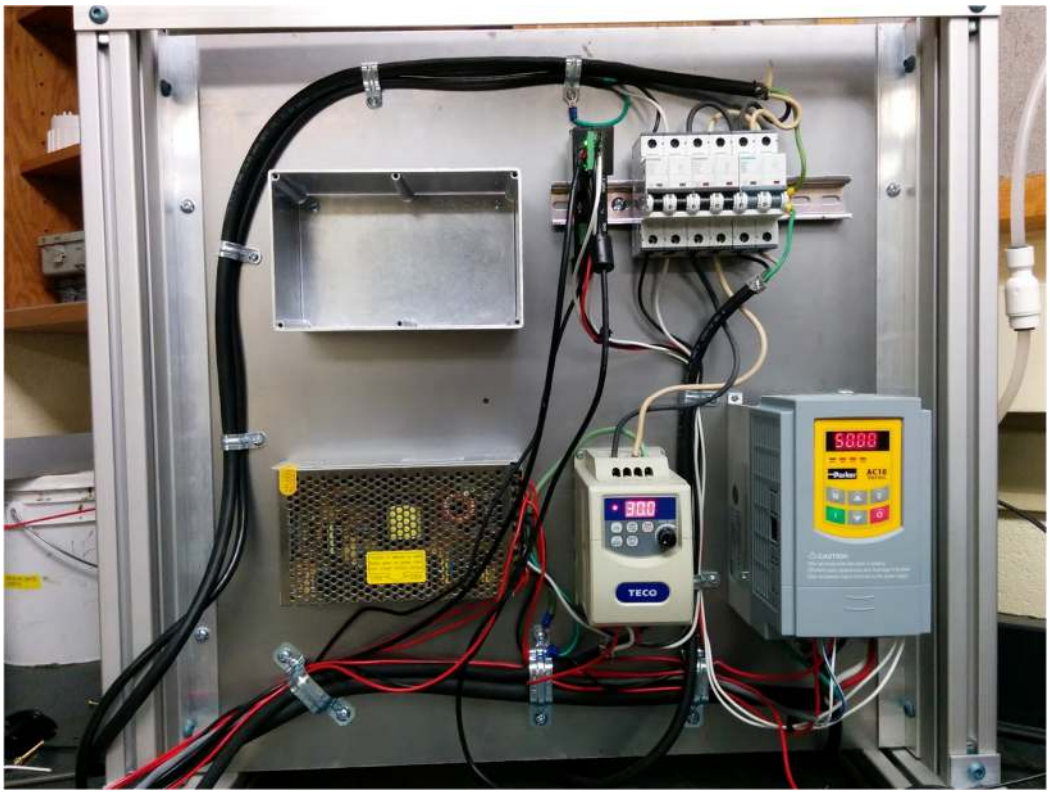

Figure 7. Electrical panel.

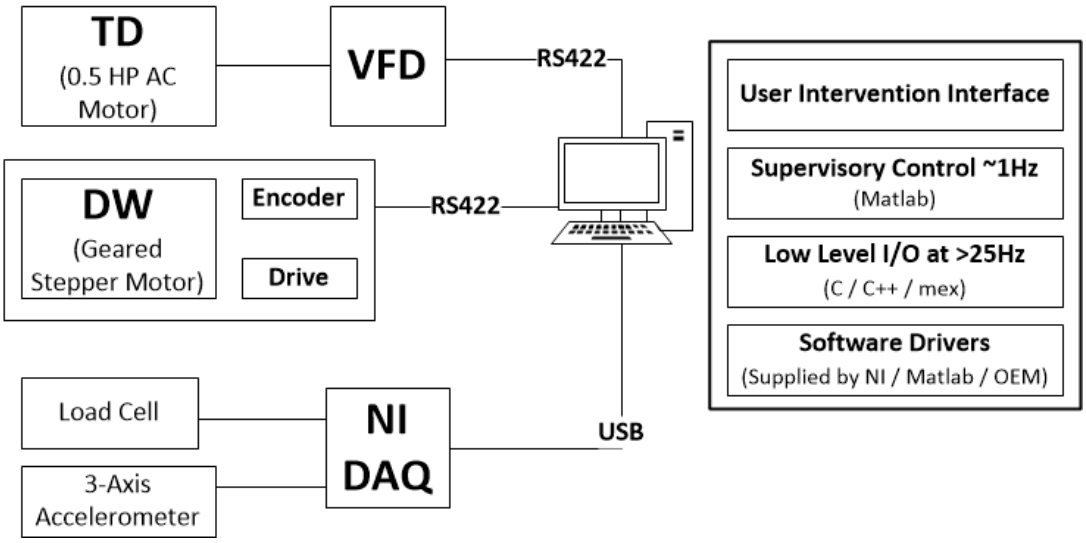

Figure 8. Control architecture.

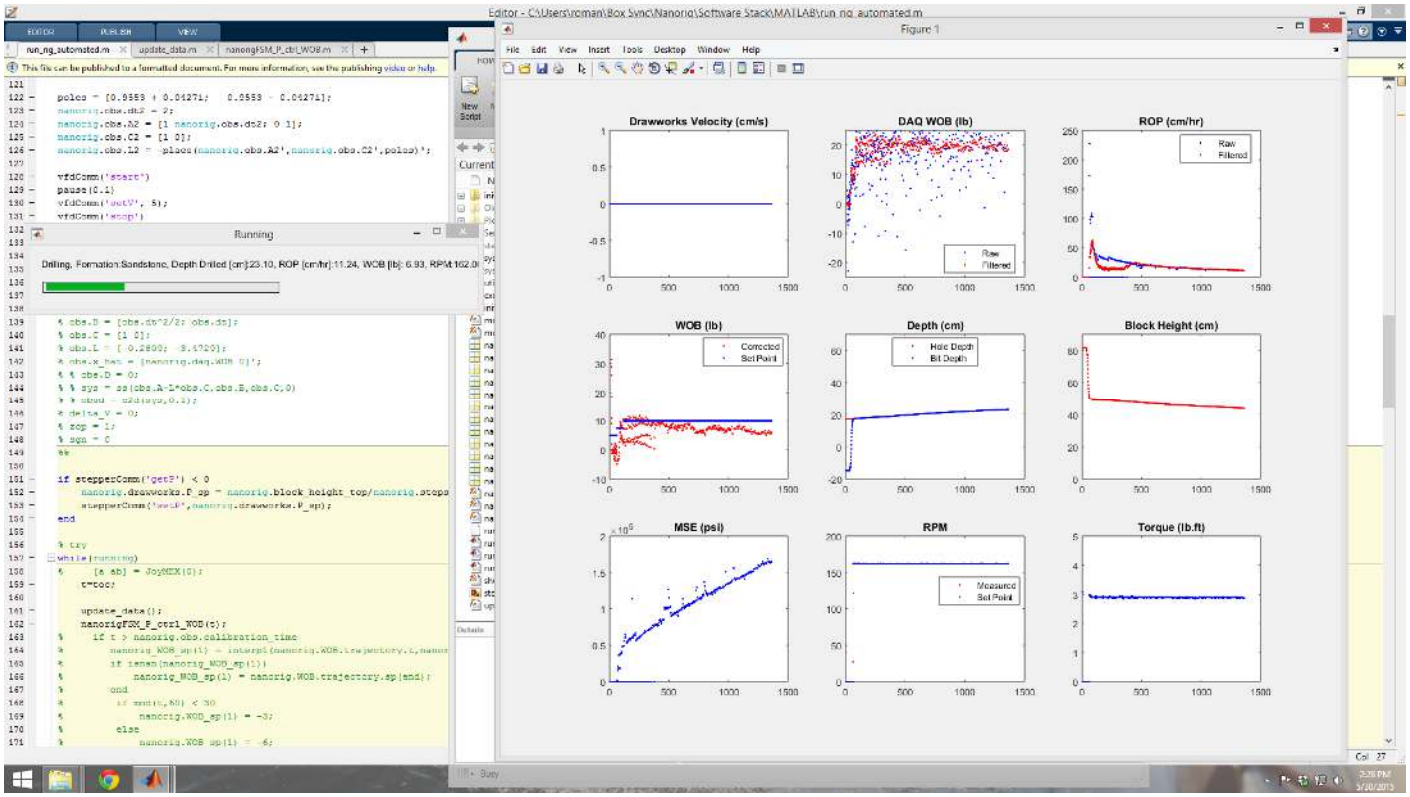

Figure 9. Basic user interface showing drilling data and a system status.

Drilling Performance

A series of drilling tests, both during competition trials and interspersed practice drilling, resulted in a slew of drilling data, allowing the performance of each subsequent drilling session to greatly improve. In the initial drilling test, conducted on May 15th, a total of 2.38 cm were drilled in 3 hours, resulting in a remarkably low ROP of 0.8 cm/hr. Controller parameters were chosen to be overly cautious, including pulling off bottom and waiting everytime weight on bit exceeded a certain value, 10 lbs in this case. This condition was triggered frequently, thus a majority of the time was spent off bottom. Block height and bit depth are shown in **Figure 10**. Also, at this time, the control parameter for weight on bit was draw works velocity, which proved to be ineffective.

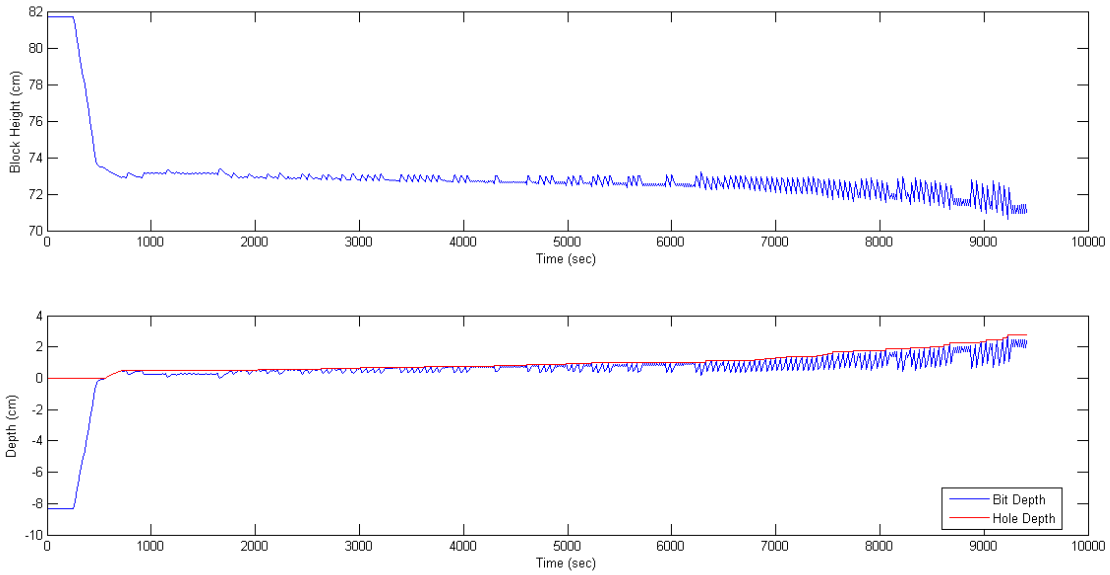

Figure 10. Block height and bit depth for the first drilling test.

Subsequent tests allowed improvements in the supervisory control and driver stack to be deployed, with the primary improvement being a move from velocity control to position control on the drawworks. This allowed for an effective sliding mode controller to be deployed for weight on bit control. At every time instant,the controller computes the relative position commanded to the stepper,

$$\Delta x = \eta \, sign(WOB_{sp} - \widehat{WOB})$$

where η is a constant gain, WOB_{sp} is the weight on bit set point and $\widehat{WOB}$ is filtered weight on bit. A low-pass filter with a 3 Hz cut-off frequency was used to obtain a smooth reading of weight on bit, given the very noisy load cell reading. A correction factor was also applied to the filtered weight on bit based on the current depth; this was necessary due to the bending moment generated in the load cell, which was observed to vary with top drive position.

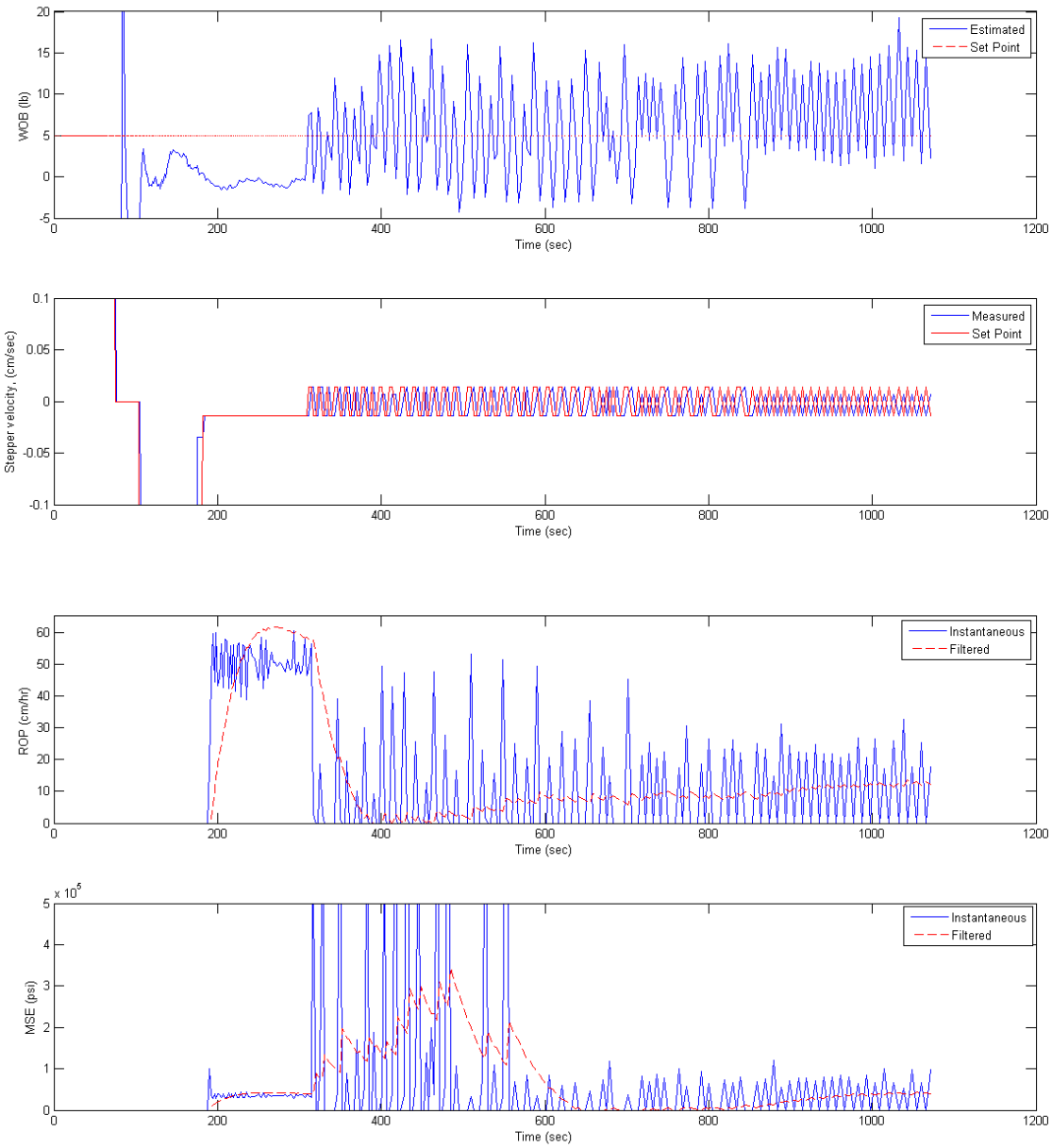

Figure 11. WOB, draw works velocity, ROP and MSE for the second test.

The final test occurred on May 30th where drilling transitioned from a sandstone layer into a granite layer. Formation detection was accomplished through a change in ROP – drilling rates in the sandstone ranged from 8-30 cm/hr based on drilling parameters (rpm and weight on bit), so a ROP threshold of 5 cm/hr was chosen to signify granite. The transition was detected immediately, both by the human observers and by the control system. The system was able to successfully drill 3.5 mm into the granite before the drillstring failed due to fatigue from significant lateral vibrations from the bit. Drilling data during the sandstone section is presented in **Figure 12** and for the transition from sandstone to granite in **Figure 13**.

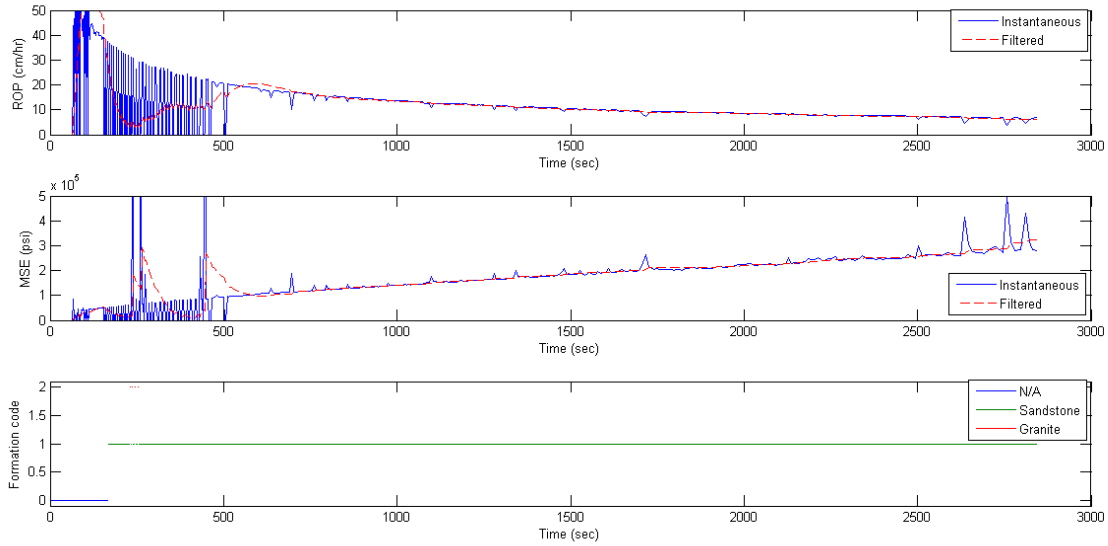

Figure 12. ROP, MSE and formation detection for the first part of the final test through sandstone.

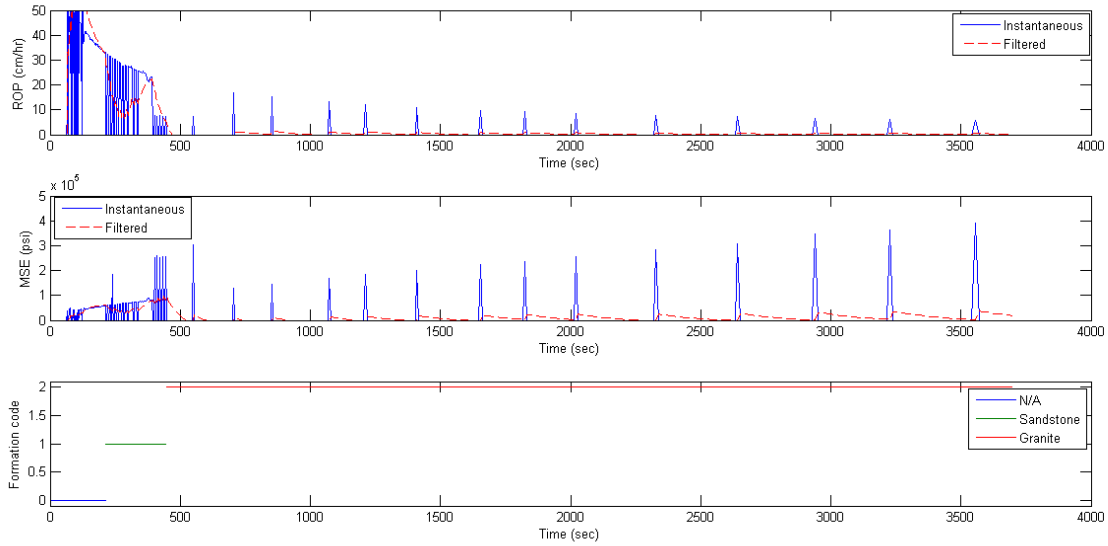

Figure 13. ROP, MSE and formation detection for the second part of the final test where granite was encountered.

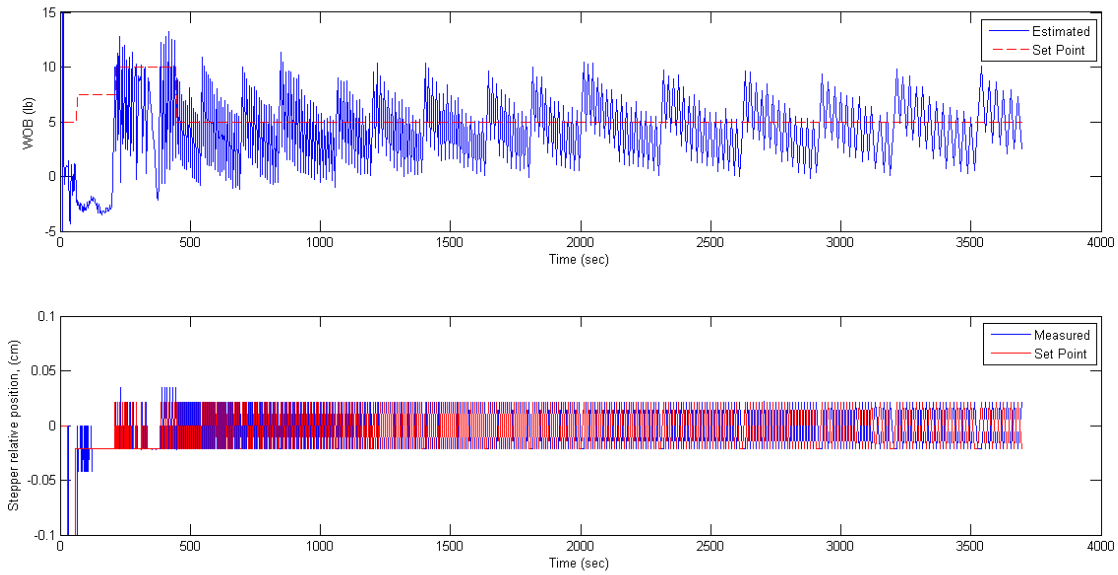

Figure 14. WOB and draw works relative displacement for the second part of the final test.

Sliding mode control was used again for weight on bit control. From the data shown in **Figure** 14, it can be seen that there was significant chatter in the drawworks displacement, and that WOB tended to drift below the set point before showing a quick burst above the set point value. These bursts coincided with the instantaneous ROP spikes visible in **Figure 13.**

Figure 15 and **Figure 16** show lateral acceleration data collected during the final test. Discarding the initial peaks in the data (up to the 500-second mark), which correspond to the drillstring tripping in and tagging bottom, we can see that the X-axis lateral acceleration through the granite has larger amplitudes than the ones recorded while drilling the sandstone. It should be noted that granite was drilled at 190 RPM, while the sandstone at only 162 RPM, which may explain the increased lateral vibration in the granite section.

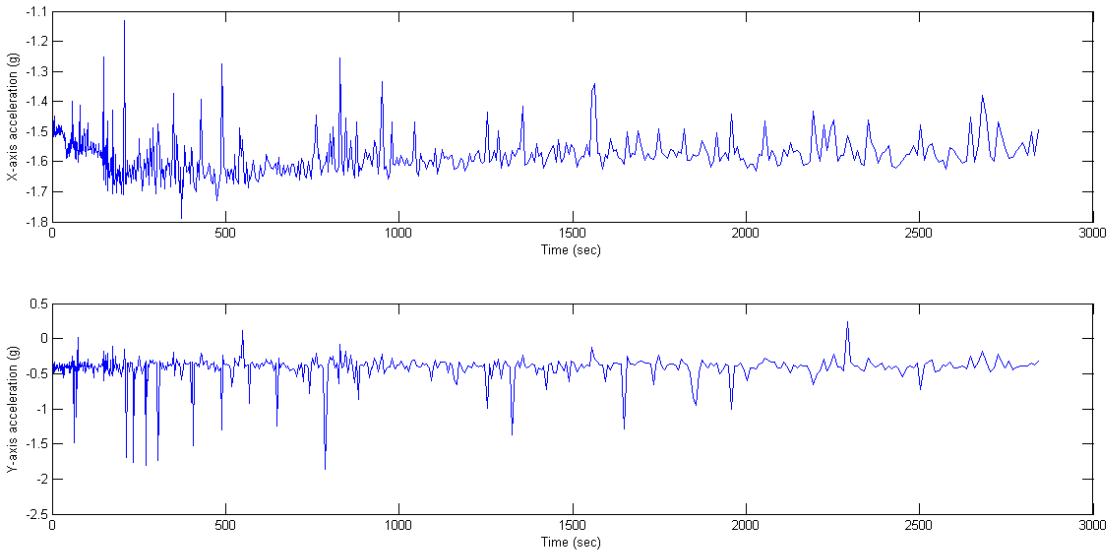

Figure 15. Accelerometer data for first part of the final test.

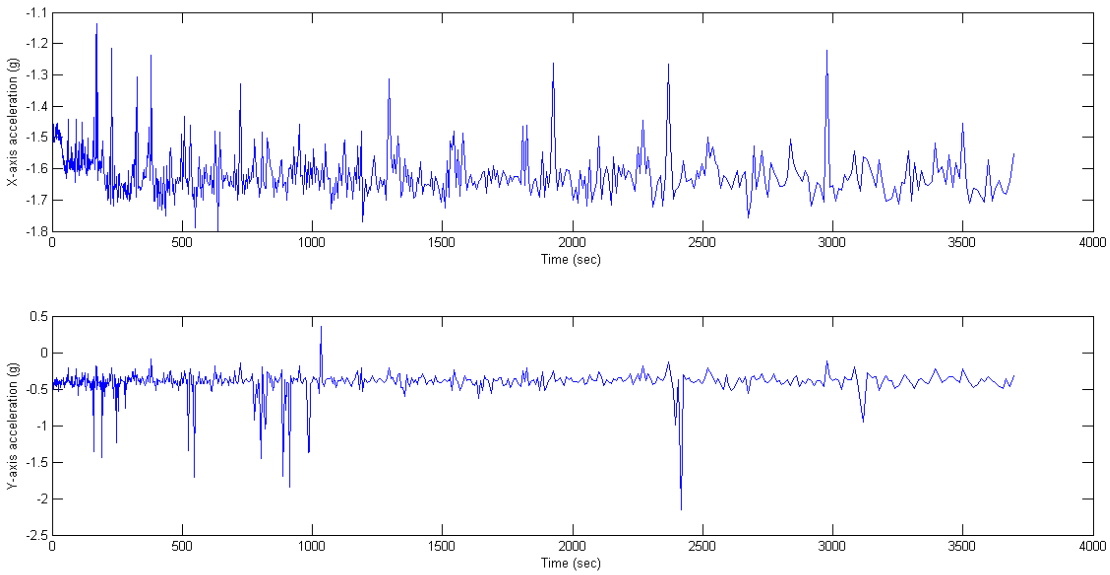

Figure 16. Accelerometer data for second part of the final test.

Visual inspection of the wellbore (**Figure 17**) at the end of the drilling test revealed a whirl pattern, more pronounced at the top of the wellbore. While acceleration data was not recorded in the early tests, lateral vibrations were observed throughout the testing. Despite the whirl, the borehole was fairly straight, and gauge rods indicated an average hole diameter of 1.25” for the first 8 inches of hole and a diameter of 1.125” for the subsequent 3.875 inches, as well as a 0.125” nipple at the bottom of the well (this was generated while drilling the granite). The total depth of the wellbore stands at 12” (30.48 cm).

Figure 17. Top view of final wellbore.

Future Work

The limitations of direct computer control over interactive protocols with the stepper and VFDs were quickly encountered during the design of the supervisory control system, and an upgrade to PLC control will occur in the near future to streamline low level control, especially for maintenance of weight-on-bit. For high-level control, the team will look into implementing more advanced, model-based control methodologies (Harris et al., 2014), as well as data-centric control architectures, where feedback control is supported by sensor data validation and event detection modules (Ambrus et al., 2015). The modular frame design will also be utilized in creating an automatic rig skidding system to allow the rig to drill multiple holes with minimal human intervention.

The Drilling and Rig Automation Group also maintains a state-of-the-art Real-Time Collaboration Center (RTCC) with the ability to stream real time data. A future data acquisition upgrade on the rig, housed in an adjacent wet lab, will bring live streaming data to the RTCC and will allow students to monitor and control rig operation to gain exposure to real-time data monitoring and control.

Conclusions

Over the course of six months, a group of students successfully designed, built and programmed a fully autonomous laboratory scale drilling rig complete with a closed loop circulation system. The final system successfully drilled through a 30-centimeter section of sandstone and 3.5 mm through granite before the competition-supplied drillstring failed due to fatigue. The control system successfully utilized sliding mode control for weight on bit control and implemented formation change detection through ROP changes.

Acknowledgements

The nanoRIG team gratefully acknowledges the help of the entire Drilling and Rig Automation Group at the University of Texas at Austin, including our advisors Drs. Pradeep Ashok, Mitch Pryor and Eric van Oort, and students Douglas Adams and Yang Zhou. The Drilling Fluids and Cementing labs are also greatfully acknowledged, especially Besmir Buranaj Hoxha. Many members of the Department of Petroleum Engineering were also pivotal in the project's success, including Glen Baum and Gary Miscoe for logistical and electrical support, and Daryl Nygaard and Mark Smith for tireless machining support.

References

Ambrus, A., Pournazari, P., Ashok, P., Shor, R., and van Oort, E. (2015, March). Overcoming Barriers to Adoption of Drilling Automation: Moving Towards Automated Well Manufacturing. In *SPE/IADC Drilling Conference and Exhibition.* Society of Petroleum Engineers.

Budynas, R., Nisbett, K. (2014), Shigley's Mechanical Engineering Design, McGraw-Hill Series in Mechanical Engineering,

Campbell F. C. (2008), Elements of Metallurgy and Engineering Alloys, ASM International.

Esmaeili, A., Elahifar, B., Fruhwirth, R. K., and Thonhauser, G. (2012, January). Experimental evaluation of real-time mechanical formation classification using drill string vibration measurements. In *SPE Annual Technical Conference and Exhibition* (pp. 8-10). Society of Petroleum Engineers.

Ersoy, A. (2003). Automatic drilling control based on minimum drilling specific energy using PDC and WC bits. *Mining Technology*, *112*(2), 86-96.

Gere J. and Goodno B., (2008). Mechanics of Materials, 7th ed., Cengage Learning.

Harris. M.W., Acikmese B. and van Oort, E. (2014, October). LMI Based Control of Stick-Slip Oscillations in Drilling. In *Proceedings of ASME Dynamic Systems and Control Conference.*

Khulief, Y. A. and Al-Sulaiman, F. A. (2009). Laboratory investigation of drillstring vibrations. *Proceedings of the Institution of Mechanical Engineers, Part C: Journal of Mechanical Engineering Science*, *223*(10), 2249-2262.

Lund, J., Cooley, C., Gonzalez, J. and Sexton, T. (2009). Laboratory drill rig for PDC bearing and cutter development. *Diamond Tooling Journal,* 20-24.

Yahr, G.T. (1997), Fatigue design curves for 6061-T6 Aluminum, *Journal of Pressure Vessel Technology* (119).

Appendix A: Torsional Shock Load Calculations

From Newton's 2nd law for rotational motion:

$$T = I\frac{d\omega}{dt}$$

where $I = 0.00287\ kg \cdot m^2$ is the top drive inertia, T is torque and ω is angular velocity.
Integrating the above relation, we get

$$\int_{t_1}^{t_2} T dt = I\int_{\omega_1}^{\omega_2} d\omega$$

$$\rightarrow T_{avg}\Delta t = I\Delta\omega$$

Assuming the RPM drops from 340 to zero in $2 \times 10^{-4} s$, this results in

$$\left|T_{avg}\right| = 0.00287 \times \frac{340}{2 \times 10^{-4}} \times \frac{2\pi}{60} = 511\ N \cdot m$$

Appendix B: Calculations for Bending and Shear of Guide Rods

The problem geometry can be set up as beam fixed at both ends with point load *P* applied at the bearing. In the sketch below, point **A** is the top end and **B** is the bottom end.

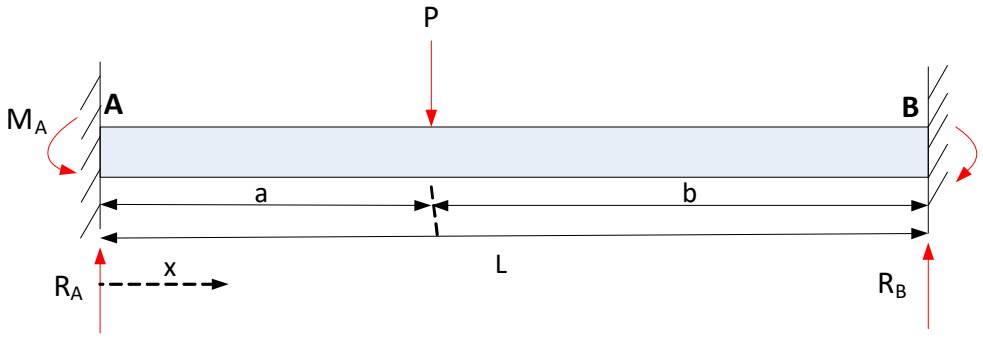

Figure 18. Guide Rod Free Body Diagram.

From the Euler-Bernoulli beam equation, we can relate the bending moment (*M)* to the deflection (*v*):

$$M = -EI\frac{d^2v}{dx^2}$$

By applying the boundary conditions at the ends ($v_A = v_B = 0,\ v'_A = v'_B = 0$) , together with the force/moment equilibrium equations, we can solve the statically indeterminate problem to find the reactions at the end points (Gere and Goodno, 2008),

$$R_A = \frac{Pb^2(L+2a)}{L^3}; R_B = \frac{Pa^2(L+2b)}{L^3}; M_A = \frac{Pab^2}{L^2}; M_B = \frac{Pa^2b}{L^2}$$

Shear force distribution:

$$V(x) = \begin{cases} \frac{Pb^2(L+2a)}{L^3}, & 0 \le x < a \\ -\frac{Pa^2(L+2b)}{L^3}, & a \le x < L \end{cases}$$

Bending moment distribution:

$$M_z(x) = \begin{cases} \frac{Pb^2(L+2a)}{L^3}x - \frac{Pab^2}{L^2}, & 0 \le x < a \\ \frac{P[b^2(L+2a)-L^3]}{L^3}x - \frac{Pab^2}{L^2} + Pa, & a \le x < L \end{cases}$$

The maximum shear force and bending moment will be experienced at the end nearest to the load application point. Assume a<b (the case where a>b effectively leads to the same results, except the point of maximum shear and bending is at the other end of the rod):

$$V_{max} = V(x=0) = \frac{Pb^2(L+2a)}{L^3}; M_{max} = M_z(x=0) = -\frac{Pab^2}{L^2}$$

To find the location of load *P* where the rod will experience the absolute maximum shear force and bending moment, we can set the derivatives of V_{max} and M_{max} with respect to *b* (distance from the top drive to the rig floor) to zero. Writing $a = L - b$, we have

$$\frac{dV_{max}}{db} = \frac{d}{db}\left[\frac{Pb^2(3L-2b)}{L^3}\right] = \frac{P}{L^3}(6bL - 6b^2) = 0 \rightarrow b = L$$

$$\frac{dM_{max}}{db} = \frac{d}{db}\left[\frac{P(L-b)b^2}{L^2}\right] = \frac{P}{L^2}(2bL - 3b^2) = 0 \rightarrow b = \frac{2L}{3}$$

$$V_{max}|_{b=L} = P\ ;\ M_{max}|_{b=\frac{2L}{3}} = -\frac{4PL}{27}$$

In practice, *b* will always be less than *L* due to the end stop position, so this V_{max} value is very

conservative.

Now we can relate these worst-case scenario shear force and bending moments to stresses. The bending stress at an arbitrary point on the rod cross-section is

$$\sigma_b = -\frac{M_z y}{I_z};$$

where I_z is the area moment of inertia about the bending axis and y is vertical coordinate along the cross-section. The shear stress at a point on the rod cross-section is

$$\tau = \frac{V Q_z}{I_z w}$$

where Q_z is the first moment of the area (maximum for a cut made at the centroid of the cross-section),and w is the cross-section width.

$$\sigma_{b,max} = -\frac{M_{max} h}{2I_z};\ \ \tau_{max} = \frac{V_{max} Q_{max}}{I_z w}$$

For a circular cross-section with radius r,

$$I_z = \frac{\pi}{4} r^4;\ Q_{max} = \frac{2}{3} r^3, w = h = 2r$$

$$\rightarrow \sigma_{b,max} = \frac{4Pab^2}{L^2 \pi r^3}; \tau_{max} = \frac{4Pb^2(L+2a)}{3L^3 \pi r^2}$$

$$\sigma_{b,\max}\big|_{b=\frac{2L}{3}} = \frac{16PL}{27\pi r^3};\ \tau_{max}\big|_{b=L} = \frac{4P}{3\pi r^2}$$